

Warm-Cold Magnetic Field Correlation in the LHC Main Dipoles

L. Bottura, M. Buzio, L. Deniau, V. Granata, L. Li, T. Pieloni, S. Sanfilippo,
W. Scandale, E. Todesco, C. Vollinger, E. Wildner

Keywords: Magnetic measurement, LHC Cryodipoles, Warm-cold correlation

Summary

We present the result of the analysis of warm-cold correlation on measured integrated dipole field strength, magnetic length and harmonics for the first 31 cryodipoles measured. This activity is of high importance to qualify sampling strategies and reduce the number of cold tests. The correlations have simple linear form, and are characterized by the r.m.s. of the warm-cold offset. We report the r.m.s. distance computed for beginning and end of injection conditions, and nominal field. The quality of the correlation, indicated by the r.m.s. of the distance between cold and warm conditions, is best for nominal conditions, degrading by at most a factor 2 at end of injection. In addition we examine the correlation of the geometric harmonics, which is as good as for nominal conditions, and discuss the features of the distribution of the warm-cold differences using the example of the normal sextupole. The present sample of data is still compatible with a single normal distribution, i.e. it is not possible to distinguish multimodal behaviour.

1. Introduction

The field and field errors of the LHC cryodipoles are measured systematically in warm conditions during the production process, in industry on collared coils as well as assembled cold masses, and at CERN in cold conditions corresponding to accelerator operation. One of the main objectives of these measurements is to verify that the field errors associated with the coil geometry of the magnets *as-built* are within specified bounds so that they are suitable for the installation in the LHC [1, 2].

This control and qualification process is heavily based on correlations established so far between the field measured in warm conditions and the corresponding values at injection and nominal field, in cold conditions. In practice the control limits for the magnet production in industry are adjusted based on these *warm-cold* correlations, and the production charts are compared to the control limits to identify and initiate corrective actions when necessary.

Sound warm-cold correlations are important now that the production rate is ramping-up, but also in the future in case that a sampling policy would be chosen for the cold tests. The aim of this note is to document the method used to establish and characterise warm-cold correlations for integrated dipole transfer function, T ,

magnetic length, L_m , and higher order harmonics, c_n , and to report the main results obtained so far.

Standard definitions are used for the above quantities. In addition we report the error on the integral dipole strength, b_1 , defined as follows:

$$b_1 = 10^4 \left(\frac{\left| \int_{L_{magnet}} B_1(x) dx \right|}{B_1 dL_{reference}} - 1 \right) \quad (1)$$

i.e. the deviation of the integral dipole strength from its reference value, $B_1 dL_{reference}$, quoted in units. The reference values for the integral dipole strength $B_1 dL$ used for the calculations are given in Table 1 below. Note that linear behaviour around the reference current was assumed to recompute the reference value of $B_1 dL$ at the measurement current. This was especially necessary for warm measurements that are routinely executed between 8 A and 15 A.

Throughout this note we will refer to warm measurements using the *state* of the magnet, i.e. either *collared coil* or *cold mass*, while for cold measurements on cryodipoles we will make reference to current and time at the moment of the measurement, i.e. *beginning of injection* flat-bottom (BOI), *end of injection* flat-bottom (EOI) and flat-top at *nominal* current (NOM).

state	collared coil	cold mass	injection (BOI and EOI)	nominal
Current (A)	10	10	760	11850
$B_1 dL_{reference}$ (T m)	0.0086097	0.010135	7.6928	119.296

Table 1. Reference value of the integrated dipole strength used to compute the dipole field error b_1 . All values are given in (T m) at the current quoted.

2. Magnets tested and data sources

The analysis of this note is based on 31 magnets cold-measured and analysed by July 2003, for a total of 62 apertures. The list of the magnets measured is given in **Appendix I**. The sample is largely biased, as it contains 19 Alstom magnets (10xx series), 4 Ansaldo magnets (20xx series) and 8 Noell magnets (30xx series).

The data was extracted from the on-line magnetic database (user interface <http://sma.cern.ch>) that provides a view to the warm measurement results (collared coil and cold mass) a direct access to the cold measurement data (beginning and end of injection and nominal) and to the geometric component of the field errors. Only integral harmonic (including body and ends) were considered in the analysis.

For magnets 1002 and 3013 the cold mass data was missing and these magnets are hence excluded in the statistics of the correlations with cold measurements results. Furthermore it was found in the analysis that the collared coil measurements of

aperture 1 of the magnet 1017 are most probably affected by a sign error on the skew multipoles. This error was identified by outliers in the scatter plot of a2 and a4, and was corrected (sign inverted) before proceeding with the statistical analysis.

3. Correlation analysis method

We have considered for the analysis that the generic warm-cold correlation between a quantity x measured in warm or cold condition is given by the linear relation:

$$x^{cold} = f_x x^{warm} + \Delta_x \quad (2)$$

where superscripts *cold* and *warm* indicate the measurement conditions, the factor f_x is a linear warm-cold scaling and the constant Δ_x is a warm-cold offset, both pertaining to the quantity x as indicated by the subscript.

Several possibilities exist for the choice of the optimal values of f_x and Δ_x . For all quantities examined here it is in principle possible to determine theoretical values for the scaling factor and for the offset. While, however, the scaling factor f_x can be predicted rather accurately, the offset Δ_x may be related to construction parameters that are not completely in control. Alternatively, it would be possible to establish both the scaling factor and the offset from a linear fit of the experimental data reported on a warm-cold scatter plot. The drawback of this approach is that the resulting correlation laws lack a physical basis and would be adversely affected by measurement outliers that cannot be identified easily. In our analysis we have chosen a mixed approach, fixing the scaling factor and using the offset as a free fitting parameter. The scaling factor was chosen based on a case-by-case inspection of the most important effects, as described below.

For the comparison of warm cold mass and cold cryodipole data we have taken a scaling factor equal to one for both the field and the harmonics. This corresponds to assuming that the change in coil geometry due to cool-down generates only an offset in the harmonics. Indeed, cool-down effects have been shown to be negligible for the harmonics, and small for the integrated main dipole transfer function for which the coil radius reduction (increasing B_l) and the coil length reduction (reducing integrated strength) partially compensate [3]. In this case the correlations for the field quantities are:

$$T^{cold} = T^{cold-mass} + \Delta_T \quad (3)$$

$$c_n^{cold} = c_n^{cold-mass} + \Delta_{cn} \quad (4)$$

For the analysis of the correlation of magnetic length of warm cold mass and cold cryodipole the dominating effect is expected to be thermal shrinkage between room temperature and operating conditions. An integrated thermal contraction coefficient of -0.3% results in a scaling coefficient of 0.997. In this case we have taken for the analysis the following expression:

$$L_m^{cold} = 0.997 L_m^{cold-mass} + \Delta_{Lm} \quad (5)$$

For what regards the correlation of warm collared coil and cold cryodipole data, the main effect to consider is the absence of the iron yoke in the collared coil. The iron causes an increase of the field strength and a change of field homogeneity. The average measured increase of the dipole strength is a factor 1.18, which agrees well with the expected factor for the addition of a shaped iron yoke to a bare collared coil [4]. The relation among the integral transfer function of collared coil and cold cryodipole used for the analysis is hence:

$$T^{cold} = 1.18 T^{collared-coil} + \Delta_T \quad (6)$$

For the harmonics, the iron contribution produces both an offset and a scaling factor through the change in the dipole strength. The scaling for the harmonics is in principle a function of the harmonic order, as the iron contributes differently to low- and high-order harmonics. For simplicity we have chosen a single scaling factor, equal to the inverse of the scaling factor chosen for the dipole transfer function, i.e. 1/1.18, leading to the following correlation:

$$c_n^{cold} = 0.85 c_n^{collared-coil} + \Delta_{cn} \quad (7)$$

Finally, the magnetic length of the collared coils has been correlated to that of cold cryodipoles using the same relation as for cold masses, i.e.:

$$L_m^{cold} = 0.997 L_m^{collared-coil} + \Delta_{Lm} \quad (8)$$

To quantify warm-cold correlations quality we have fitted scatter plots of cold vs. warm measured data with the expressions above. An example of a typical result is reported in Fig. 1 for the scatter plot of cold b_3 data at end of injection vs. warm b_3 data from collared coils.

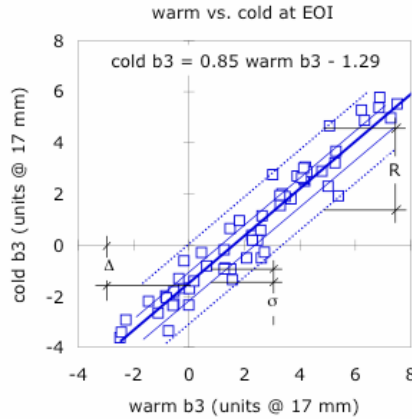


Figure 1. Example of warm-cold correlation analysis, illustrating the meaning of the correlation parameters (scaling factor and offset) and correlation quality indicators. The data selected for this example is normal sextupole data, b_3 , measured on the collared coil (warm) and at the end of injection (cold).

The results of the fit are the warm-cold offset and the r.m.s. of the warm-cold distance, measured along the y axis, indicated with σ . In addition we have systematically computed the min-max range of the above distance, indicated below with R . In the case reported in Fig. 1 we have $\Delta = -1.29$ units @ 17 mm, a r.m.s. of $\sigma = -0.72$ units @ 17 mm, and a range $R = 3.09$ units @ 17 mm.

4. Results at beginning of injection and nominal conditions

We have used the procedure above to determine the warm-cold offset, the r.m.s. and the range of the warm-cold distance for warm measurements taken on the collared coil and on the cold masses vs. measurements at the beginning of injection and at nominal field. These are the two operating points that are considered for specification of the production values. The numerical results are reported in Tables. 2 and 3 for the low-order harmonics and the allowed high-order harmonics. The same results have been reported in Figs. 2 and 3 where we have plotted the warm-cold offset for the harmonics considered, and we have added bars indicating the 1σ ranges.

	beginning of injection - collared coil			beginning of injection - cold mass		
	Δ	σ	R	Δ	σ	R
b1	-2.36	5.36	25.43	-2.23	4.48	22.12
b2	1.69	0.34	1.83	-1.64	0.36	1.15
a2	-0.20	0.37	1.79	-0.13	0.38	2.39
b3	-2.94	0.42	1.81	-7.49	0.38	1.68
a3	-0.10	0.10	0.64	-0.07	0.12	0.46
b4	0.05	0.06	0.38	-0.03	0.04	0.21
a4	-0.03	0.11	0.71	0.00	0.12	0.84
b5	0.98	0.13	0.62	0.98	0.13	0.65
b7	-0.36	0.04	0.20	-0.35	0.04	0.18
b9	0.18	0.02	0.08	0.16	0.02	0.07
b11	0.04	0.01	0.07	0.03	0.01	0.04

Table 2. Summary of the systematic warm-cold offset Δ , the r.m.s. of the warm-cold distance σ and the min-max warm-cold range R as obtained analysing data taken at beginning of injection and measured on the collared coil (left) or the cold mass (right).

	nominal - collared coil			nominal - cold mass		
	Δ	σ	R	Δ	σ	R
b1	-3.97	6.20	30.33	-3.92	4.87	23.41
b2	0.21	0.36	1.73	-3.13	0.41	1.64
a2	-0.23	0.25	1.41	-0.16	0.16	0.74
b3	4.40	0.34	1.40	-0.11	0.33	1.46
a3	-0.11	0.11	0.67	-0.09	0.12	0.45
b4	0.26	0.06	0.27	0.18	0.03	0.13
a4	-0.02	0.06	0.33	0.02	0.04	0.20
b5	-0.29	0.09	0.45	-0.30	0.07	0.30
b7	-0.01	0.03	0.14	0.00	0.02	0.09
b9	-0.06	0.01	0.08	-0.08	0.01	0.04
b11	0.01	0.01	0.04	0.01	0.01	0.03

Table 3. Summary of the systematic warm-cold offset Δ , the r.m.s. of the warm-cold distance σ and the min-max warm-cold range R as obtained analysing data taken at nominal conditions and measured on the collared coil (left) or the cold mass (right).

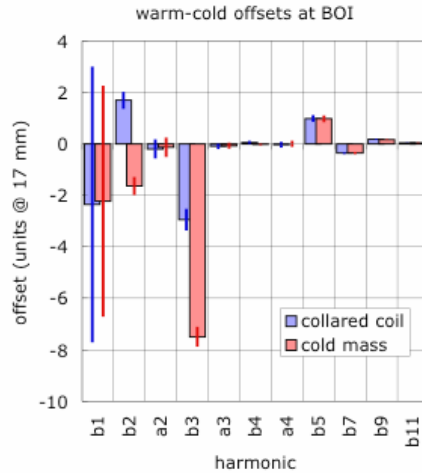


Figure 2. Summary of the systematic warm-cold offset Δ for selected low order and allowed high order harmonics obtained analysing data measured at beginning of injection vs. data from collared coil or cold mass (solid bars). The ranges (lines) at the top of each bar represent the r.m.s. of the warm-cold distance σ .

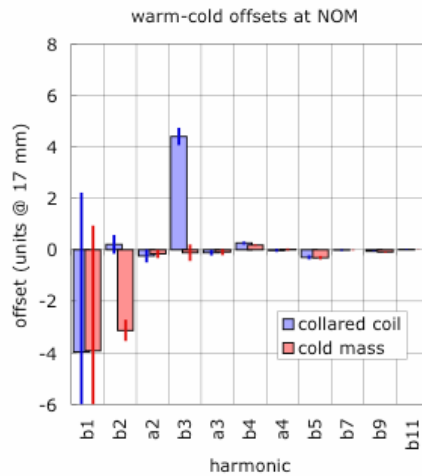


Figure 3. Summary of the systematic warm-cold offset Δ for selected low order and allowed high order harmonics obtained analysing data measured at nominal conditions vs. data from collared coil or cold mass.

As a general remark we notice that both the r.m.s. and the range are large for the main dipole error b_1 . This error is caused by the uncertainty in the determination of the magnetic length as well as in the measurement of the body field in warm conditions, as discussed later. For the other harmonics the correlations σ computed for data at injection and nominal vs. both collared coil and cold mass are relatively small. To be remarked the modest increase in σ on the allowed harmonics b_3 and b_5 between nominal and injection conditions, which is due to the additional spread that is associated with the contribution of persistent currents.

4.1 Transfer function, magnetic length, dipole strength error

The following Figs. 4 through 6 report the scatter plot of warm and cold data for the integrated transfer function, the magnetic length and the dipole error b_1 , showing in detail the correlation of the data available. As already discussed above, the correlation is relatively poor. This is particularly evident in Fig. 6 for b_1 where the warm-cold distance has a spread that is comparable to the spread in the production (i.e. the ellipse of the cloud of points has similar sizes in the two quadrant directions).

The same result is obtained also from the integral transfer function and the magnetic length. The values of Δ , σ and the ranges for T and L_m are reported in Tables. 4 and 5. Indeed, once normalised to the reference value of the transfer function and magnetic length, it is clear that a comparable spread is present on all three quantities.

This result hints to one of the sources of the error, namely a known issue in the warm measurement systems used in industry for which the measurement of the longitudinal position is not precisely calibrated. A random positioning error of the order of 1 cm could explain a substantial part of the σ obtained from the correlation analysis. In addition the dipole measurement resolution in the straight part also has a r.m.s. error of the order of a few units, which adds to the σ of the correlation. Activity is in progress to improve the calibration and the precision of the positioning of the warm measurement systems.

	collared coil			cold mass		
	Δ	σ	R	Δ	σ	R
T beginning of injection	0	0.0065	0.0293	0	0.0040	0.0170
T nominal	-0.057	0.0075	0.0342	-0.057	0.0045	0.0190

Table 4. Summary of the systematic warm-cold offset Δ , the r.m.s. of the warm-cold distance σ and the min-max warm-cold range R as obtained analysing integral transfer function data taken at beginning of injection and nominal vs. measured data on the collared coil (left) or the cold mass (right). All results reported in Tm/kA. The reference value of the transfer function is approximately 10.1 Tm/kA.

	collared coil			cold mass		
	Δ	σ	R	Δ	σ	R
L_m beginning of injection	-92	7.1	37.4	-35	4.6	18.8
L_m nominal	-90	7.1	39.3	-34	5.0	21.3

Table 5. Summary of the systematic warm-cold offset Δ , the r.m.s. of the warm-cold distance σ and the min-max warm-cold range R as obtained analysing magnetic length data taken at beginning of injection and nominal vs. measured data on the collared coil (left) or the cold mass (right). All results reported in mm. The reference value of the magnetic length is 14300 mm.

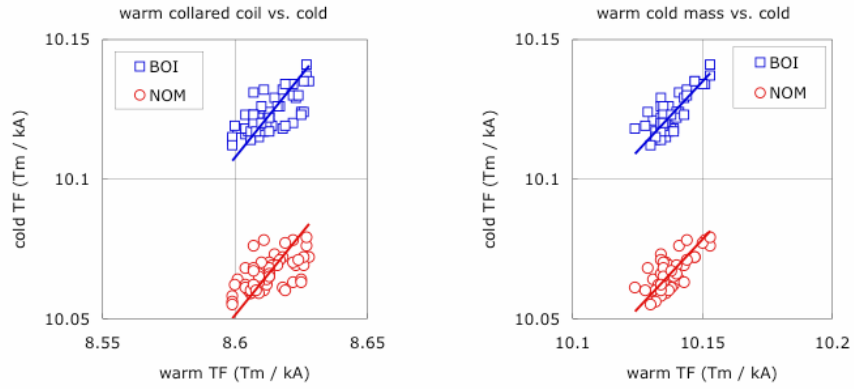


Figure 4. Scatter plot of dipole transfer function as measured in cold conditions at beginning of injection or nominal conditions vs. warm conditions on the collared coil (left) or the cold mass (right).

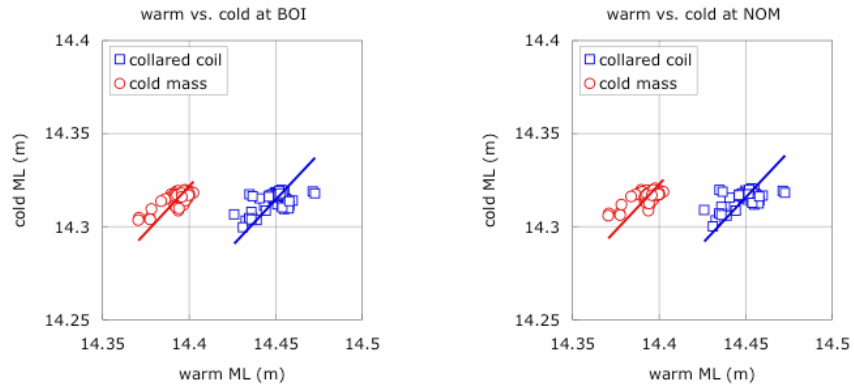


Figure 5. Scatter plot of magnetic length as measured in cold conditions at beginning of injection (left) or at nominal (right) vs. warm conditions on the collared coil or the cold mass.

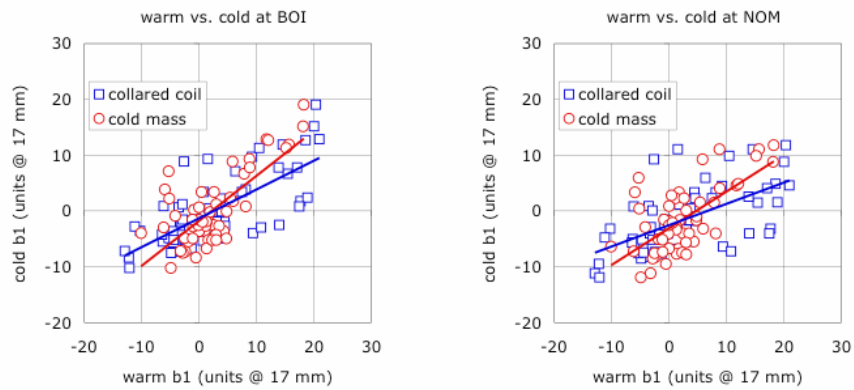


Figure 6. Scatter plot of warm-cold correlations for the integrated dipole strength error. Cold conditions at beginning of injection (left) or at nominal conditions (right) are plotted vs. the warm measurements on the collared coil or cold mass. The lines are solely intended to guide the eye.

4.2 Higher order harmonics

The situation for the warm-cold correlation on the higher order harmonics (quadrupole and higher) is much better than on the dipole error, as shown by the scatter plots reported in Figs. 7 through 10. For the normal sextupole b_3 in particular the value of σ is between 0.34 (correlation between data for collared coil and nominal conditions) and 0.42 units @ 17 mm (correlation between data for collared coil and beginning of injection conditions), which is a very good result. Note also in the scatter plot that the slopes of the best fits of collared coil data are consistently smaller than those of cold mass data, as expected by the scaling with the dipole field implied by Eqs. (4) and (7). Finally, the two apparently *anomalous* points in the correlation among cold normal quadrupole and collared coil data (in Fig. 8, square symbols), can be explained as they correspond to the two apertures of magnet 1002. This magnet, together with magnet 1005, had a different iron geometry by virtue of which a different warm-cold offset would be expected (1005 was not cold measured and hence does not appear in the plot).

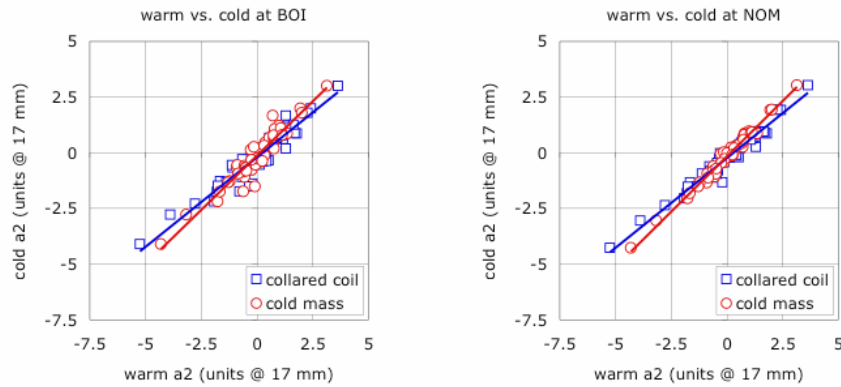


Figure 7. Scatter plot of warm-cold correlations for the integrated skew quadrupole error. Cold conditions at beginning of injection (left) or at nominal conditions (right) are plotted vs. the warm measurements on the collared coil or cold mass.

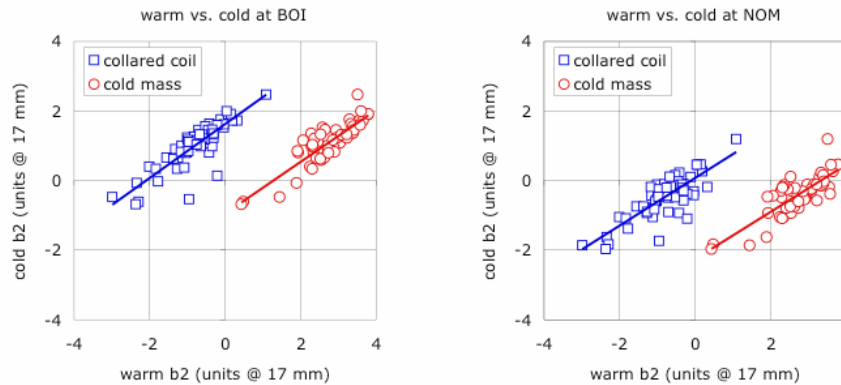


Figure 8. Scatter plot of warm-cold correlations for the integrated normal quadrupole error. Cold conditions at beginning of injection (left) or at nominal conditions (right) are plotted vs. the warm measurements on the collared coil or cold mass.

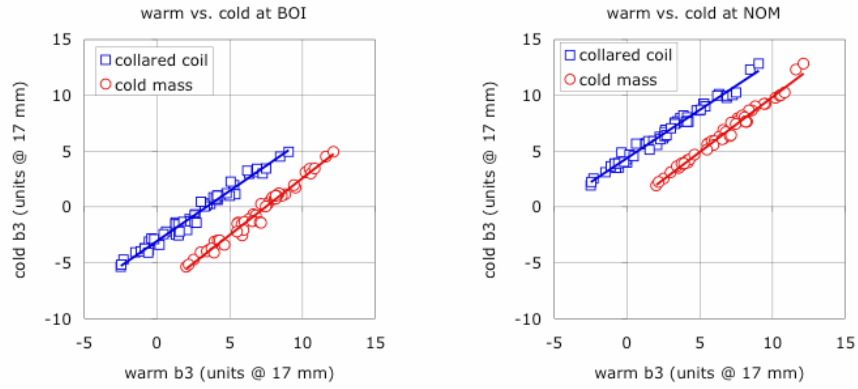


Figure 9. Scatter plot of warm-cold correlations for the integrated normal sextupole error. Cold conditions at beginning of injection (left) or at nominal conditions (right) are plotted vs. the warm measurements on the collared coil or cold mass.

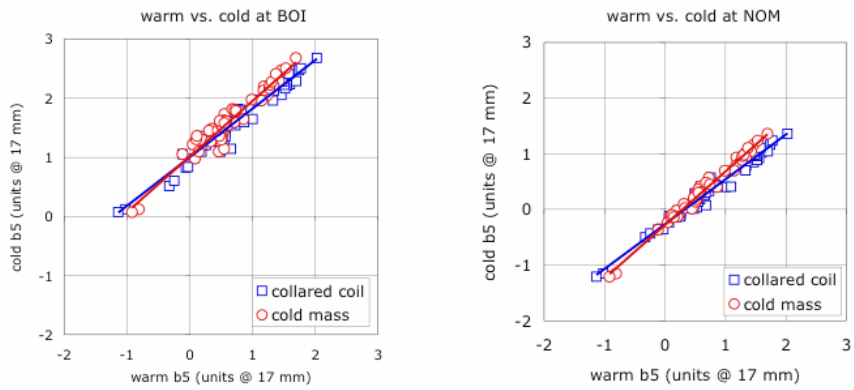


Figure 10. Scatter plot of warm-cold correlations for the integrated normal decapole error. Cold conditions at beginning of injection (left) or at nominal conditions (right) are plotted vs. the warm measurements on the collared coil or cold mass.

5. Results at end of injection

Between beginning and end of injection the field drifts by an amount that depends mainly on cable electrical characteristics and powering history. The above parameters do not contribute to warm field quality. Therefore we expect that the warm-cold correlations to field measured at the end of injection is degraded with respect to the results discussed previously. This is confirmed by the results reported in Table 6 and summarised in Fig. 11, where the end of injection conditions refers to a 1000 s injection flat-bottom following a 30 minutes flat-top pre-cycle at nominal current (11850 A).

The effect is particularly evident on the normal sextupole, which is the harmonic most affected by the injection decay, see the scatter plot of Fig. 12, to be compared to the scatter plot in Fig. 9. The σ of the warm-cold correlation increases from 0.42 units @ 17 mm at the beginning of injection to 0.72 units @ 17 mm at the end of injection. This increase can be attributed to an uncorrelated additional random effect of about 0.58 units @ 17 mm, which is of the same order of the r.m.s. on the measured sextupole decay. Note that the r.m.s. on the sextupole decay is expected to increase by approximately 40 % in the case of long pre-cycles (typically more than 1 hour flat-top) and long injections (typically more than 1 hour flat-bottom), as would be the case for the routine operation of the LHC. This would eventually result in a maximum projected warm-cold σ of about 0.9 units @ 17 mm on b_3 .

	end of injection - collared coil			end of injection - cold mass		
	Δ	σ	R	Δ	σ	R
b2	1.67	0.33	1.90	-1.66	0.40	1.34
a2	-0.22	0.46	2.05	-0.17	0.45	2.38
b3	-1.29	0.72	3.09	-5.90	0.63	2.86
a3	-0.07	0.13	0.96	-0.05	0.13	0.53
b4	0.06	0.07	0.39	-0.02	0.05	0.30
a4	-0.02	0.14	0.62	0.02	0.15	0.75
b5	0.73	0.19	0.80	0.74	0.18	0.83
b7	-0.33	0.04	0.20	-0.32	0.04	0.18
b9	0.16	0.02	0.12	0.14	0.02	0.11
b11	0.04	0.02	0.12	0.03	0.02	0.10

Table 6. Summary of the systematic warm-cold offset Δ , the warm-cold standard deviation σ and the min-max warm-cold range R as obtained analysing data taken at the end of a 1000 s simulated injection plateau, and measured on the collared coil (left) or the cold mass (right).

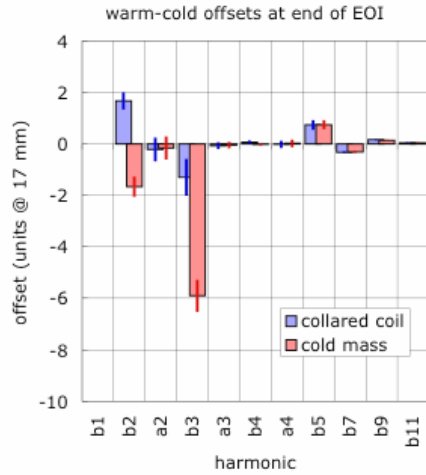


Figure 11. Summary of the systematic warm-cold offset Δ for selected low order and allowed high order harmonics obtained analysing data measured at end of injection vs. data from collared coil or cold mass.

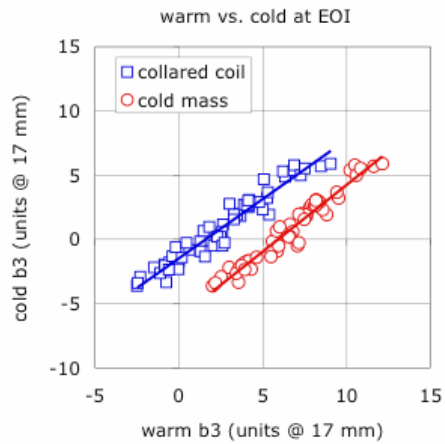


Figure 12. Scatter plot of warm-cold correlations for the integrated normal sextupole error. Cold conditions at end of a simulated 1000 s injection are plotted vs. the warm measurements on the collared coil or cold mass.

6. Correlation of warm and cold geometric harmonics

Warm measurements are essentially detecting deviations of the coil geometry from its nominal size. This is indeed the main source of field errors in warm conditions. In cold conditions the field errors have additional, large contributions from persistent currents (at injection) and iron saturation (at nominal). The field errors are dominated by coil geometry only at intermediate excitation, i.e. around 5 kA for the LHC dipoles.

We have tested the quality of the correlation of warm measurements to geometric harmonics derived from cold measurements taken at 5 kA, expecting the correlation to improve. The results, reported in Table 7 and in graphical form in Fig. 13, substantiate the above statement. In particular, the correlation with warm cold mass data is excellent on all harmonics, demonstrating that the effect of the change of coil geometry due to cool-down is small, and results (apart for b_2) in a negligible warm-cold offset.

	geometric - collared coil			geometric - cold mass		
	Δ	σ	R	Δ	σ	R
b2	1.74	0.29	1.63	-1.60	0.45	1.35
a2	-0.13	0.24	1.41	-0.06	0.15	0.68
b3	4.28	0.32	1.26	-0.22	0.36	1.58
a3	-0.11	0.11	0.65	-0.09	0.12	0.46
b4	0.07	0.05	0.27	-0.01	0.03	0.11
a4	-0.02	0.06	0.28	0.02	0.04	0.18
b5	-0.18	0.08	0.39	-0.19	0.06	0.28
b7	-0.01	0.02	0.13	0.00	0.02	0.08
b9	-0.02	0.01	0.08	-0.04	0.01	0.05
b11	0.02	0.01	0.05	0.01	0.01	0.03

Table 7. Summary of the systematic warm-cold offset Δ , the warm-cold standard deviation σ and the min-max warm-cold range R as obtained analysing geometric multipoles deduced from cold measurements at 5 kA, and multipoles measured on the collared coil (left) or the cold mass (right).

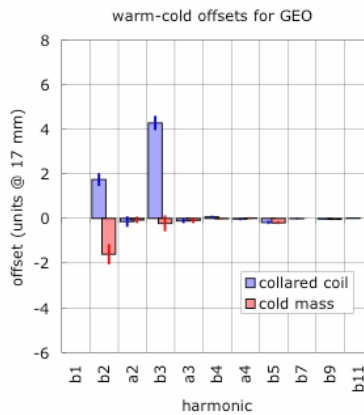


Figure 13. Summary of the systematic warm-cold offset Δ for selected low order and allowed high order harmonics obtained analysing geometric harmonics from cold measurements vs. data from collared coil or cold mass.

7. Distributions

As a last item in this analysis, we have examined the distribution of the warm-cold data around the correlation line. The aim of this analysis was to see whether the warm-cold differences are due to a purely random process (which would lead to a normal distribution around the warm-cold offset), or whether an additional set of systematic biases is present in the population.

For this analysis we have taken the histogram of the difference between the measured data in cold conditions and the warm data scaled by the appropriate warm-cold scaling factor f_x , i.e. using the ideal correlation line as given by Eqs. (2) through (8) without the offset. A practical example for this calculation is shown in Fig. 14 (on the left) for the specific case of the normal sextupole at the end of injection, where the difference is indicated with Δb_3 . The result of the histogram calculation leads to the distribution of magnet apertures as a function of the difference Δb_3 also shown in Fig. 14 (on the right). The average of the distribution corresponds to the warm-cold offset Δ reported earlier (the zero intersect of the correlation line), and the variance corresponds to the square of the r.m.s. σ of the warm-cold correlation.

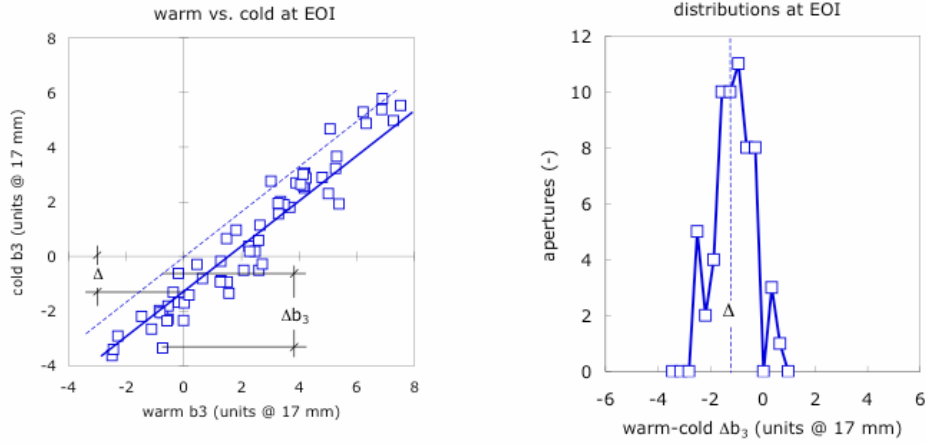


Figure 14. Schematic of the calculation of the warm-cold distributions in the specific case of the normal sextupole at end of injection. The data on the scatter plot (left) is processed to obtain the warm-cold correlations. An histogram of the differences Δb_3 , produces a distribution (right) centered on the warm-cold offset Δ (zero intersect of the correlation line) and with the warm-cold variance σ^2 .

To illustrate the general results we have selected the case of the normal sextupole b_3 , for which we have computed the distribution of the differences:

$$\Delta b_3 = b_3^{cold} - 0.85 b_3^{collared\ coil} \quad (9)$$

for the correlation of cold data (beginning and end of injection, nominal) to warm collared coil data, and:

$$\Delta b_3 = b_3^{cold} - b_3^{cold\ mass} \quad (10)$$

for the correlation of cold data to warm cold mass data. The distributions obtained for the warm-cold correlations are reported in Figs. 15 through 17. The results obtained for the small number of samples available (62 apertures) are not easy to interpret. Although the distribution appears to have multiple peak features, especially for the sextupole at nominal conditions in Fig. 16, the values of the higher order moments of the distribution (skewness and kurtosis), reported in Table 8, are still compatible with a normal distribution. We recall that the expected limit for the skewness of a sample of 62 apertures on a normal distribution is 0.31, while for the kurtosis the limit is 0.62 and only large differences (i.e. factors) with respect to these expected values indicate deviations from a normal distribution.

warm	cold	skewness	kurtosis
collared coil	beginning of injection	-0.24	-0.16
	end of injection	-0.08	-0.19
	nominal	0.29	-0.20
cold mass	beginning of injection	-0.32	1.89
	end of injection	0.02	1.30
	nominal	-0.48	1.06

Table 8. Third order moment (skewness) and fourth order moment (kurtosis) of the distribution of the warm-cold differences around the correlation line of the measured b_3 values.

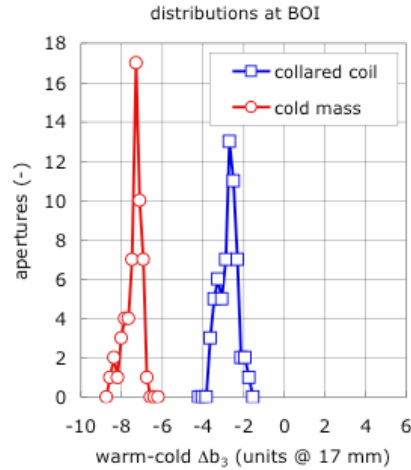


Figure 15. Distribution of the warm-cold difference for the normal sextupole as measured in cold conditions at beginning of injection vs. the data from collared coil (squares) or cold mass (circles). The histogram was obtained from the correlation plot of Fig. 9 (right).

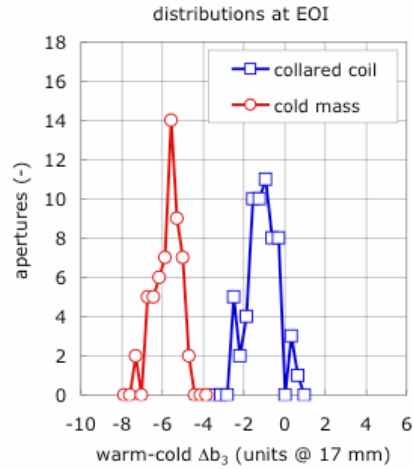


Figure 16. Distribution of the warm-cold difference for the normal sextupole as measured in cold conditions at the end of injection vs. the data from collared coil (squares) or cold mass (circles). The histogram was obtained from the correlation plot of Fig. 12.

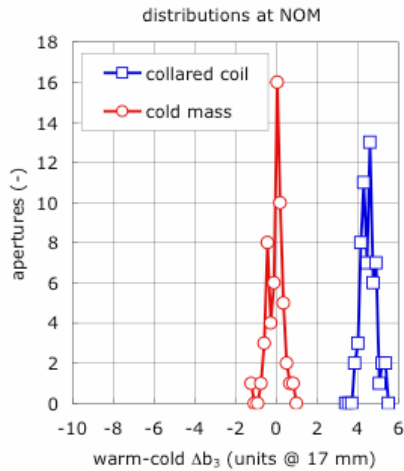


Figure 17. Distribution of the warm-cold difference for the normal sextupole as measured in cold conditions at nominal conditions vs. the data from collared coil (squares) or cold mass (circles). The histogram was obtained from the correlation plot of Fig. 9 (right).

8. Conclusions

We have reviewed in this note the warm-cold correlations derived from the magnetic measurements of the first 31 cryodipoles. We have quantified the results obtained in terms of the r.m.s. of the distance between the cold measurement and the ideal correlation line with the warm measurement, σ . The correlation is much better on higher order harmonics than on main field (integral dipole transfer function and magnetic length). For the harmonics a very good correlation is found between warm measurement and geometric harmonics at cold, as well as with harmonics at nominal conditions. The quality of the correlation is less satisfactory at beginning of injection, due to the variability of persistent current effects, and degrades further at end of injection, due to the field decay. In practice, these effects are of relevance only for the normal sextupole component.

To give a statement on whether the quality of the correlation is sufficient it is useful to compare the correlation σ to the specification of the width of the windows used for accepting magnets [2]. We have considered in particular two windows:

- the allowable half-range for the running average of the installed magnets, obtained as half the size of the smallest intersection of the windows that define *green* dipoles at all operating conditions, i.e. dipoles for which direct and blind installation is possible;
- the allowable standard deviation for the running average, obtained from the difference between the definition of a *green* and a *yellow* dipole, i.e. a dipole for which the running average shall be verified before installation.

In order to have a good control of the production and installation the correlation σ should be small compared to both windows considered above. The comparison is shown in Figs. 18 and 19 for the collared coil data, upon which fast feed-back is required. We see that the σ of the warm cold correlation for harmonics is in all cases smaller than both the allowable range and the allowable standard deviation of the running average. The only exception is the dipole strength, for which the correlation σ is larger than the standard deviation allowed for the running average. In this case a sufficient control of the variation of integral dipole strength may not be guaranteed.

As discussed in the text, we believe that the origin of this large spread is to be attributed to a measurement artifact that is being addressed at present. Similarly, a calibration of the warm measurement system is in progress to establish a warm-cold correlation for the field direction, for which very scattered data is available to date.

More insight in the warm-cold correlations can be gained by inspection of the distribution of the measured points around the best fit correlation line. At present, with a sample of 62 apertures, the value of the higher order moments of the warm-cold difference are still compatible with a normal distribution.

This activity, the update and study of warm-cold correlations, will be pursued as it is relevant to qualify any sampling strategy aiming at reducing the number of cold tests.

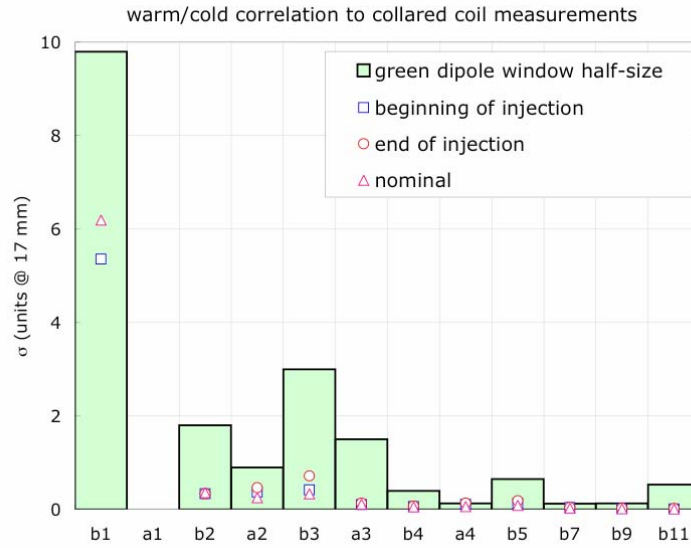


Figure 18. Comparison of the correlation σ and the allowable range of the running average for *green* dipoles for low order harmonics and high order allowed harmonics. Warm data taken from collared coil measurements.

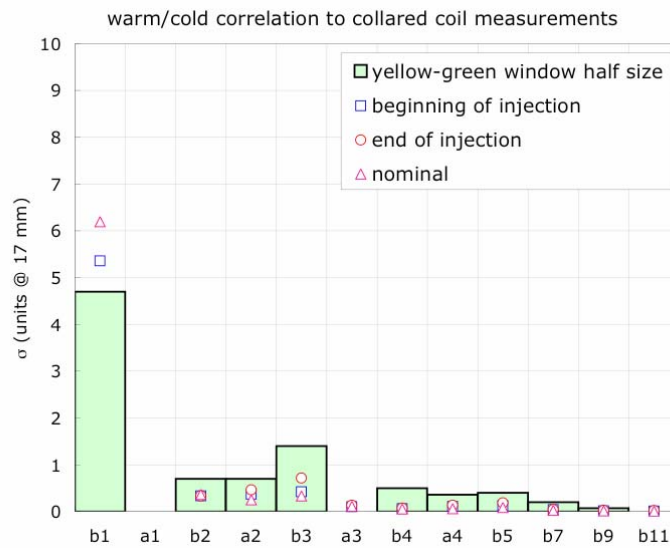


Figure 19. Comparison of the correlation σ and the standard deviation of the running average, defining the difference between *green* and *yellow* dipoles, for low order harmonics and high order allowed harmonics. Warm data taken from collared coil measurements.

9. References

- [1] O. Bruning, S. Fartoukh, "Field Quality Specification for the LHC Main Dipole Magnets", LHC-Project-Report-501, 2001.
- [2] Summary of the LHC Magnet Evaluation Board [MEB] meeting held on 21 June 2002, EDMS no: 350428 v.1.
- [3] P. Ferracin, Mechanical and magnetic analysis of the Large Hadron Collider main dipole, Ph. D. Thesis, Politecnico di Torino, 2002.
- [4] C. Vollinger, Private Communication, 2003.

10. Appendix I – List of magnets included in the analysis

The following table contains the list of magnets that were considered for the analysis presented here. For magnets 1002 and 3013 the cold mass data was missing, and thus was not considered in the calculation of the statistical indicators. For magnet 1017 the skew multipoles of Aperture 1 as measured in the collared coil are probably affected by a sign error. This data has been artificially corrected (sign inversion of skew multipoles) to remove the large mis-match particularly evident on a2 and a4.

Magnets

HCMBBRA001-01000001
HCMBBRA001-01000002
HCMBBRA001-01000003
HCMBBRA001-01000004
HCMBBRA001-01000006
HCMBBRA001-01000007
HCMBBRA001-01000008
HCMBBRA001-01000009
HCMBBRA001-01000010
HCMBARA001-01000011
HCMBARA001-01000012
HCMBARA001-01000013
HCMBARA001-01000014
HCMBBRA001-01000015
HCMBBRA001-01000016
HCMBBRA001-01000017
HCMBBRA001-01000018
HCMBBRA001-01000019
HCMBBRA001-01000024
HCMBBRA001-02000001
HCMBBRA001-02000003
HCMBBRA001-02000004
HCMBBRA001-02000006
HCMBBRA001-03000001
HCMBBRA001-03000002
HCMBBRA001-03000005
HCMBARA001-03000006
HCMBARA001-03000007
HCMBARA001-03000009
HCMBBRA001-03000011
HCMBBRA001-03000013